Available on CMS information server

**CMS NOTE 1999/014**

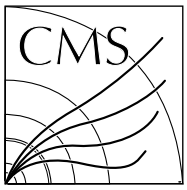


**The Compact Muon Solenoid Experiment**

# CMS Note

Mailing address: CMS CERN, CH-1211 GENEVA 23, Switzerland

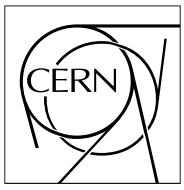


**05 Feb. 1999**

# Beam test results on $n^+$ on $n$ type silicon microstrip detectors before and after neutron irradiation

M. M. Angarano, A. Bader, D. Creanza, M. de Palma, L. Fiore, G. Maggi, S. My, V. Radicci, G. Raso, G. Selvaggi, L. Silvestris, P. Tempesta

*INFN and University of Bari, Bari, Italy*

**Abstract**

We present beam test results on AC-coupled, single-sided, $n^+$-on-$n$ type silicon microstrip detectors. We have tested the detectors before and after irradiation at a fluence of $8.3 \times 10^{13}\ n/cm^2$, at different temperatures and bias voltages. The signal-to-noise ratio, spatial resolution, charge collection and overall efficiency have been measured.

# 1 Introduction

The signal-to-noise ratio (S/N) is one of the most important parameters of silicon microstrip detectors, since it strongly affects both the detection efficiency and the spatial resolution. Therefore, the investigation of the signal-to-noise ratio at different detector working conditions (temperature, bias voltage, environmental radiation level) is of major interest in high energy experiments. The silicon microstrip detectors in the tracking system of the future CMS experiment at LHC (CERN) will be exposed to radiation up to a fluence of $\simeq 1.6 \times 10^{14}\ n/cm^2$ after 10 years of operation [1]. Due to the irradiation, several detector parameters, such as capacitance and resistance values, effective doping concentration, full depletion voltage and leakage current, will change. The modification of the capacitive coupling parameters, especially the increase of the interstrip capacitance for conventional $p^+$ on $n$ devices, causes a less effective charge coupling and an increased noise level [1, 2, 3]. The other main effect which is expected to strongly influence the noise after irradiation is the substantial leakage current increase. In addition to the signal loss and the increased noise, after a certain fluence the detector reaches type inversion, and it can require high bias voltage in order to be fully depleted. Usually, in order to avoide the anti-annealing effect and to reduce the leakage current, the detectors must be operating at low temperature, typically in the range of $-10 \div 0\,^{\circ}C$.

In this paper we investigate on the performances of $n^+$-on-$n$ type detectors, focusing our attention on signal-to-noise ratio and efficiency before and after neutron irradiation, at different operation temperatures and bias voltages. One of the main advantages of this type of detectors is that, after type inversion, they can work in partial depletion mode. After type inversion, in fact, the depletion region extends, with increasing bias voltage, from the strips side towards the $p^+$ back-plane, thus giving a sufficiently extended active area under the $n^+$ strips at bias voltages well below the full depletion value ($V_{dep}$). This feature may be crucial if the full depletion voltage cannot be reached because it exceeds the detector breakdown voltage.

# 2 Detectors description

The subject of the present study are single-sided, AC coupled detectors with $n^+$ strips implanted over a $n$ type substrate and a plain $p^+$ layer at the back, which have been produced by SINTEF [4] as prototypes for the ATLAS detector [5]. The active area of the detectors is 57.4 $mm \times$ 57.4 $mm$, the thickness is 280 $\mu m$. The total number of strips is 1025, with a pitch of 56 $\mu m$. Every second strip has a metallised read-out strip; the readout pitch is thus 112 $\mu m$. Isolation between $n^+$ strips is achieved by using the p-stop technique. The $n^+$ strips are biased through 2 $M\Omega$ polysilicon resistors, while the $p^+$ blocking strips are left floating during the operation. Coupling capacitors are obtained by 200 $nm\ SiO_2$ plus 100 $nm\ Si_3N_4$ layers grown between the implantation strips and the metallization. The main detector parameters are summarized in table 1; more details can be found in [6].

| | |
|---:|---:|
| Active Area | $57.4\,mm \times 57.4\,mm$ |
| Thickness | $280\,\mu m$ |
| Resistivity | $4 - 8\,K\Omega \cdot cm$ |
| Nr. of $n^+$ strips | 1025 |
| Nr. of read-out strips | 512 |
| $n^+$ pitch | $56\,\mu m$ |
| Read-out pitch | $112\,\mu m$ |
| $n^+$ strips width | $12\,\mu m$ |
| $p^+$ strips width | $18\,\mu m$ |
| $Al$ strips width | $8\,\mu m$ |

Table 1: Main parameters of $n^+$-on-$n$ SINTEF detectors [5].

Some of the detectors were irradiated with neutrons up to a fluence of $8.3 \times 10^{13}\ n/cm^2$ in the nuclear reactor "Tapiro" at ENEA-Casaccia Laboratory (near Rome), Italy. The irradiation was performed at room temperature and without biasing the detectors. In the period between the irradiation and the beam test the detectors were kept at a temperature $\simeq 0^{\circ}C$ to inhibit both annealing and anti-annealing effects. The current, capacitance and resistance parameters changes as a function of the neutron fluence were investigated in our previous work [2].

# 3 Experimental setup

For the test beam studies two detectors were glued together and precisely mounted on a rigid $G10$ frame. The two detectors were electrically connected. This module corresponds to a detector with $11.48\ cm$ strip lenght. The

module was connected to PreMux128 preamplifiers [7] through a pitch adapter, located in the same frame. The shaping time of PreMux128 was set to $50\ ns$ and the data were collected in not-correlated sampling mode [7]. The module was read-out by a VME-based DAQ system, described in detail in ref. [9]. In an edge region of the detector only every second read-out strip was connected to the preamplifier, while the strips in between were left floating, in order to get read-out pitch of 224 $\mu m$.

The detectors were tested in a particle beam at two subsequent times: before irradiation (october '97) and after irradiation (november '97). The measurements were performed at $15°C$, $-5°C$ and $-10°C$ for the unirradiated module and at $0°C$, $-5°C$ and $-10°C$ for the irradiated one. For low temperature runs, the detectors and the electronics were mounted inside a thermally insulated box in which cooled air was circulated. The temperature was monitored inside the box and was stable within $\pm 0.5°C$. The detector was biased through the $p$-side with a negative bias voltage ($V_p$) in a range around the depletion voltage. The full depletion voltage was evaluated from current, resistance and capacitance measurements performed in laboratory [2]. The full depletion voltage was $V_{dep} = 70\ V$ before irradiation and $V_{dep} = 110\ V$ after irradiation.

On the beam line, the module was located along a high resolution beam telescope [8]. A $100\ GeV$ muon beam was used at X5 CERN area. The trigger was defined by the coincidence of two scintillators in front of and behind the detectors. The active area of the scintillators was $2cm \times 2cm$ for the run before irradiation and $6cm \times 6cm$ after irradiation.

# 4 Analysis method

The signal on each strip was calculated event by event by a computer code described in detail in [9]. In the algorythm the signal of the $i$-th channel, $S_i$, is obtained by subracting from the raw value acquired by the ADC, $R_i$, the strip pedestal $PED_i$ and the common mode fluctuation, $CM$:

$$S_i = R_i - PED_i - CM. \tag{1}$$

The strip noise, $N_i$ is calculated as the statistical fluctuation of $S_i$, taking care not to include those events in which the strip may have been hit by a particle. Strips are identified as bad (noisy, disconnected or shorted) when the value of their noise goes outside an acceptance range. Once the signal and the noise for each strip are known, the program looks for clusters of signals on adjacent strips in order to identify the passage of a particle. First the "seeds" of the clusters are searched, looking for strips for which $S_i/N_i > T_s$ (seed $S/N$ threshold). Once at least one such strip is found, the program adds to the cluster all the adjacent strips (max. 7 on both sides of the seed strip) for which $S_j/N_j$ is greater than a new threshold value $T_a$ ($T_a < T_s$).

The candidate cluster is retained for further analysis if the number of strips $\mathcal{N}$ is not larger than 7 and the number of bad strips in the cluster does not exceed one. The cluster signal ($S_{cl}$) and noise ($N_{cl}$) are defined as:

$$S_{cl} = \sum_{i=1}^{\mathcal{N}} S_i \qquad\qquad N_{cl} = \sqrt{\sum_{i=1}^{\mathcal{N}} (N_i)^2 / \mathcal{N}}.$$

Finally, the candidate clusters are accepted if $S_{cl}/N_{cl} > T_{cl}$ (global cluster threshold). Following this procedure, more than one cluster per event can be identified; spurious clusters can be produced by noisy strips, $\delta$ electrons or accidental hits. In this case, the most energetic cluster is selected.

The optimization of the threshold values is a crucial point in the evaluation of the signal-to-noise ratios. If the thresholds are set too low, events due to noise are not discriminated. On the other hand, if the thresholds values are too high one may cut away true particles clusters. The optimum threshold values have been determined using the experimental data obtained for the detectors before irradiation, at $15°C$ and $V_p = 90\ V$. First we optimized the cluster and seed thresholds, subsequently we fixed the threshold for the adjacent strips. The distribution of $S_{cl}/N_{cl}$, shown in figure 1, clearly indicates that the noise events can be excluded by setting $T_{cl} \geq 5.2$.

Studying the behaviour of important parameters - such as $S_{cl}$, average number of clusters per event, average number of strips in a cluster, fraction of 1-, 2-, 3- and 4-strip clusters - as a function of $T_s$ and $T_{cl}$ (see figure 2) we fixed the cluster and seed thresholds at $T_{cl} = 5.2$ and $T_s = 3$.

In order to determine the optimum value of $T_a$ we looked at the fraction of clusters with even and odd number of strips; the experimental distributions are shown in figure 3. The 1- and 3-strip clusters can be attributed mainly to impacts close to a readout strip, while 2- or 4-strip clusters to impacts close to an unread strip. The relative

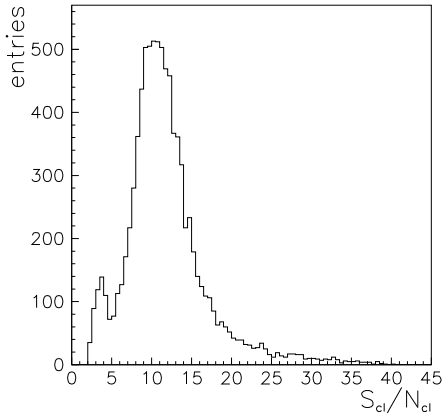


Figure 1: $S_{cl}/N_{cl}$ distribution for low threshold values: $T_{cl} = 2$, $T_s = 2$, $T_a = 1$ ($V_p = 90\ V$, $T = 15°C$, before irradiation).

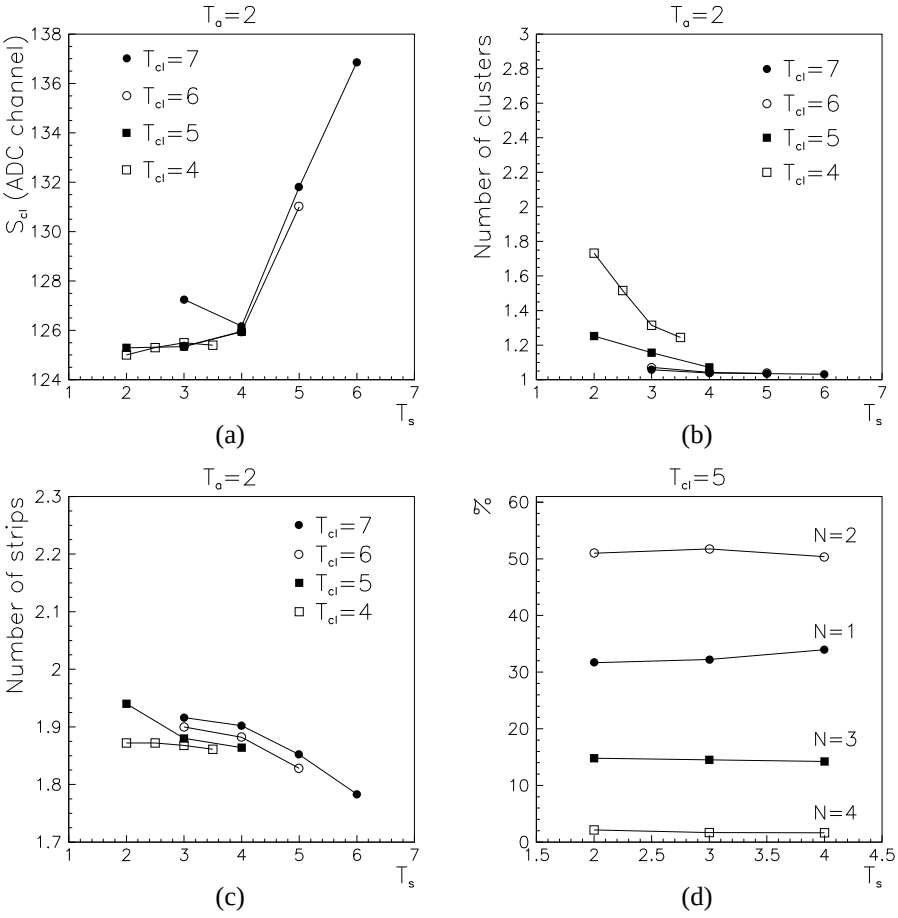


Figure 2: Average cluster signal (a), average number of clusters per event (b), average number of strips in a cluster (c) and fraction of 1-, 2-, 3- and 4-strip clusters (d) as a function of $T_s$ ($V_p = 90\ V$, $T = 15°C$, before irradiation).

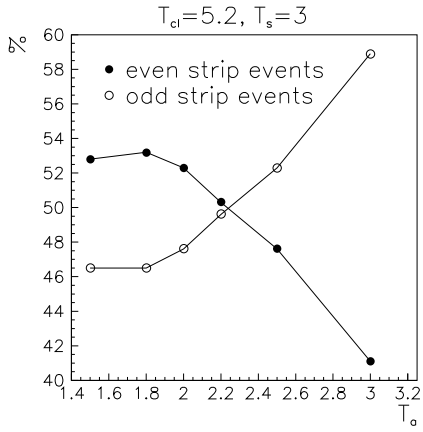


Figure 3: Fraction of clusters with odd (1 or 3) and even (2 or 4) number of strips versus the adjacent strips threshold $T_a$ ($V_p = 90\ V$, $T = 15°C$, before irradiation).

| *Temp.* | $15°C$ | $0°C$ | $-5°C$ | $-10°C$ |
|---|---|---|---|---|
| $T_{cl}$ | 5.2 | 5.4 | 5.5 | 5.7 |
| $T_s$ | 3 | 3.1 | 3.2 | 3.3 |
| $T_a$ | 1.8 | 1.9 | 1.9 | 2.0 |

Table 2: Cluster, seed and adjacent strips threshold values for different temperatures.

amount of even and odd strips clusters, being essentially determined by the strip pitch, should not change with the threshold values. We find the optimum value of $T_a$ at 1.8, the maximum cut value at which the ratio between the number of odd and even strips clusters is still constant.

In order to determine the threshold values to be used at other operation temperatures ($T$) we scaled the thresholds obtained for $15°C$: $T_{cl,s,a}(T) = T_{cl,s,a}(15°C) \cdot S_{cl}(T)/S_{cl}(15°C)$. The corresponding threshold values are listed in table 2. For the irradiated detectors the same thresholds determined for the unirradiated ones were used.

The most probable value of the Landau distributions fitting the experimental $S_{cl}$ distribution for each temperature and bias voltage value, before and after irradiation, defines the "detector signal amplitude" (figure 4-(a)). Analogously, the most probable value of the Gaussian functions fitting the various cluster noise distributions, assumed normally distributed, defines what we refer to in the following as "detector noise" (figure 4-(b)). The detector

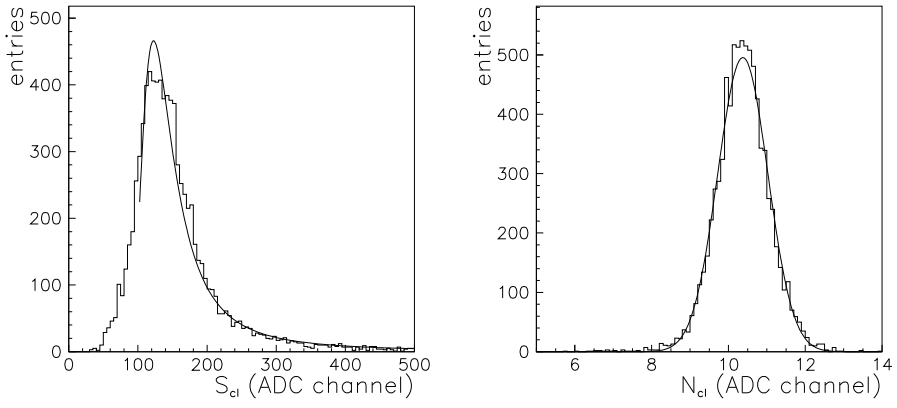


(a) (b)

Figure 4: Typical cluster signal distribution and Landau-function fit (a); typical cluster noise distribution and Gaussian-function fit (b) ($V_p = 200\ V$, $T = -5°C$, after irradiation).

signal-to-noise ratio is then defined as the ratio between the most probable values of $S_{cl}$ and $N_{cl}$.

The signal-to-noise ratio was also studied by a simulation [3], in which the detector was modeled as a network of resistors, capacitors and diodes. The parameters of the elements of the network were determined by current, resistance and capacitance measurements, performed independently from the beam test [2]. The detector model was connected to the equivalent circuit model of PreMux128, whose input transistor was tuned to have the specified noise characteristics [13]. In the simulation, we injected into a connected read-out, a not connected read-out or a non-read-out strip a charge corresponding to 22400 $e^-$, and measured the charge coupling to the input of the preamplifier and the signal amplitude at the output of the preamplifier. We also determined the noise of the detector and of the read-out electronics. The simulation took into account the noise of the preamplifier, the noise due to the leakage current and the thermal noise related to the series and bias resistors.

# 5 Experimental results

We have studied the cluster signal-to-noise ratio, the efficiency, the spatial resolution and the charge collection of the detector before and after irradiation at different temperatures and bias voltages.

## 5.1 Cluster signal-to-noise ratio

We have not observed evident change in the shape of $S_{cl}$ and $N_{cl}$ distribution before and after irradiation. Typical distributions of $S_{cl}$ and $N_{cl}$ are shown in figure 4 for the irradiated detector at $T = -5°C$ and $V_p = 200\ V$. Moreover, no appreciable increase of the number of the dead and noisy channels have been seen in the irradiated detector.

In figure 5 the signal, noise and signal-to-noise ratio bias voltage dependence for various operation temperature, before and after irradiation, is shown. Both the signal amplitude and the noise increase when the temperature decreases. This effect is mainly due to the increasing gain of the amplifier with decreasing temperature [14].

Before irradiation the signal amplitude is expected to reach its plateau value above full depletion voltage, when the depletion region reaches the strip-side and the strips get isolated. Below $V_{dep}$ no cluster signal is expected. On the contrary we found that the signal does not drop sharply below the depletion voltage (see in figure 5-(a)). This effect is explained by the fact that, in this case, the strips don't get uniformly isolated across the detector, as can be seen in figure 6. In this figure the distribution of the cluster peak position is shown at bias voltages just below (a) and above (b) full depletion; at $V_p = 60\ V$, $10\ V$ below the nominal full depletion voltage, there are regions where the detector is already active (figure 6-(a)) and clusters can thus be reconstructed. At $V_p = 70\ V$ the uniform cluster peak position distribution indicates that all the detector is active, i.e. fully depleted and with isolated strips (figure 6-(b)).

Below the depletion voltage, when the strips are not isolated, the interstrip capacitance and the load capacitance seen by the read-out electronics (which, in turn, depends on the interstrip capacitance) are high and cause high noise, as can be seen in figure 5-(b) [2].

After irradiation the detector substrate was type inverted. In a $p$-type substrate the depletion region starts growing from the strip-side when a bias voltage is applied, and the strips are already isolated at low voltage, much below full depletion voltage. As a consequence, the signal amplitude reaches the plateau value smoothly (figure 5-(d)) and the noise stays practically constant above the depletion voltage (figure 5-(e)). This effect can be better seen in figure 7 where for a given operation temperature the signal, noise and $S/N$ ratio behaviour as a function of overdepletion voltage ($V_p - V_{dep}$) before and after irradiation are directly compared.

Our results show that before irradiation the noise level can be further reduced by overdepleting the detector. This is not the case after irradiation, since the leakage current, which increases with increasing bias voltages, contributes to the noise considerably and compensates the decrease of the noise due to the smaller load capacitance.

As a consequence of the above considerations, before irradiation the signal-to-noise ratio raises sharply as the full depletion voltage is reached, and can be further increased by overdepleting the detector. After irradiation, instead, the signal-to-noise ratio starts to increase much below full depletion and shows a milder raise above the depletion voltage with respect to the unirradiated case, with irradiated detectors showing worse performances than non irradiated ones at any given overdepletion voltage value (fig. 7-(c)).

Above full depletion a $S_{cl}/N_{cl} \simeq 13$ was measured for the irradiated detectors; this value is in good agreement with those measured by the ATLAS collaboration [5].

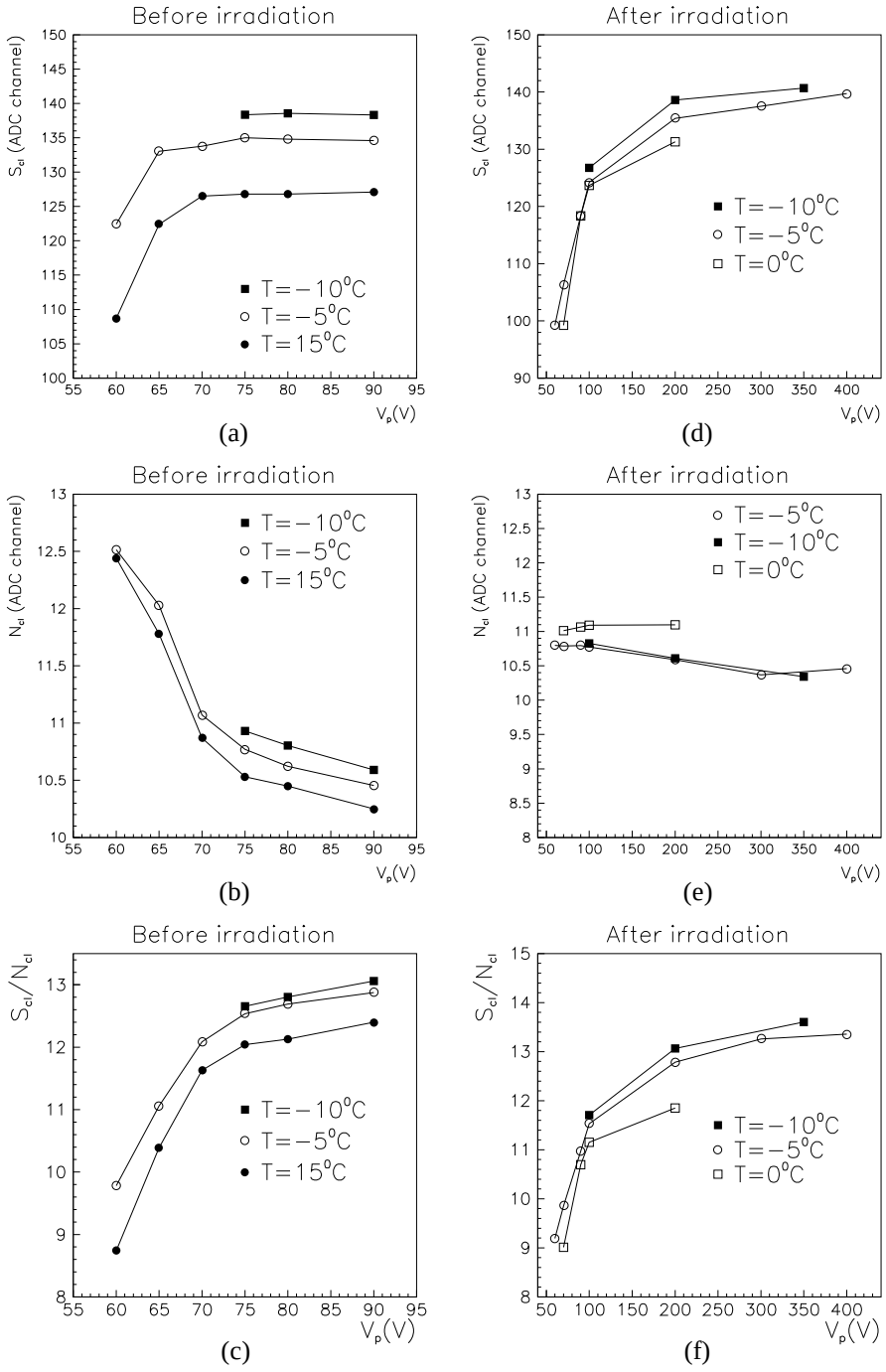


Figure 5: $S_{cl}$ (a), $N_{cl}$ (b) and $S_{cl}/N_{cl}(c)$ before irradiation; $S_{cl}$ (d), $N_{cl}$ (e) and $S_{cl}/N_{cl}$ (f) after irradiation.

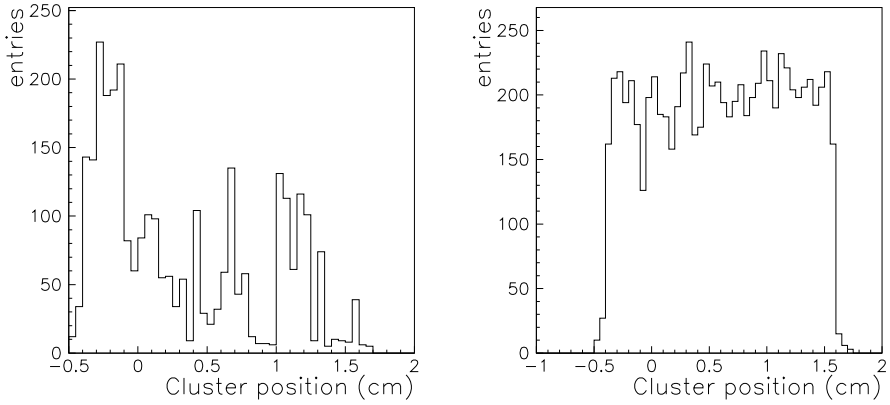


(a) (b)

Figure 6: Cluster peak position distribution before irradiation at $V_p = 60\ V$ (a) and at $V_p = 70\ V$ (b).

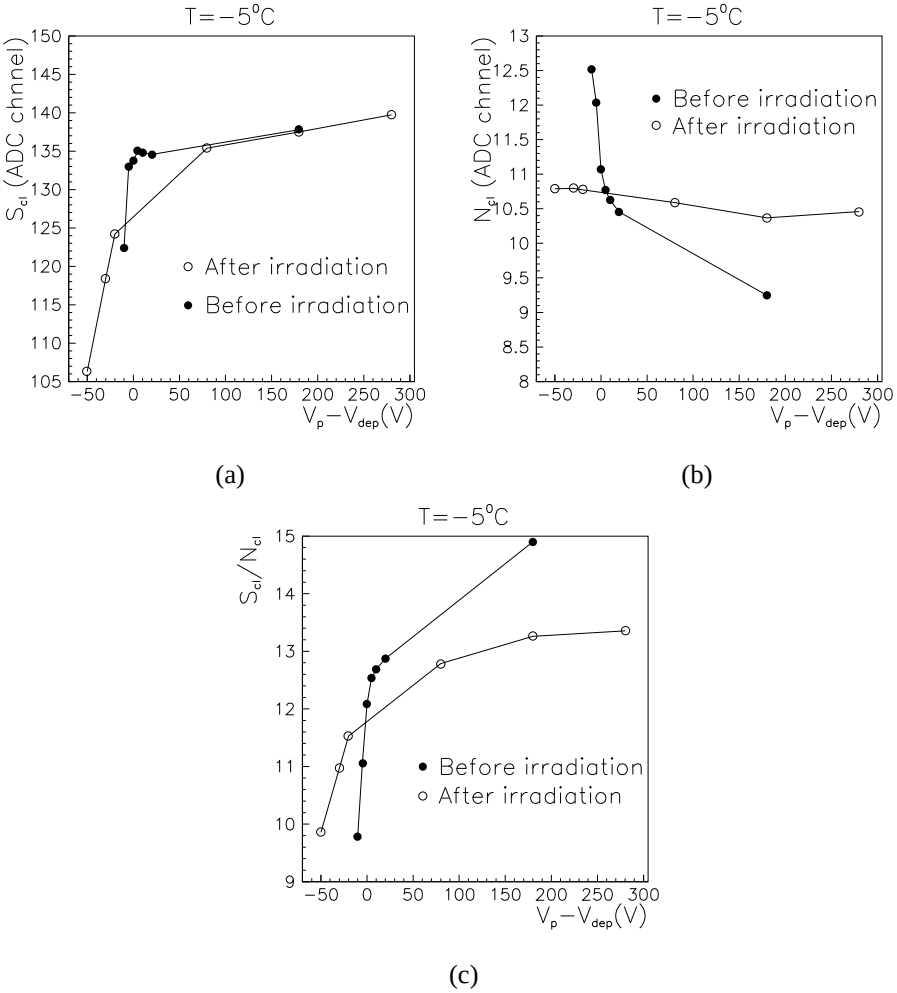


(a) (b)

(c)

Figure 7: Comparison of $S_{cl}$ (a), $N_{cl}$ (b) and $S_{cl}/N_{cl}$ (c) as a function of overdepletion voltage, before and after irradiation, at $T = -5°C$.

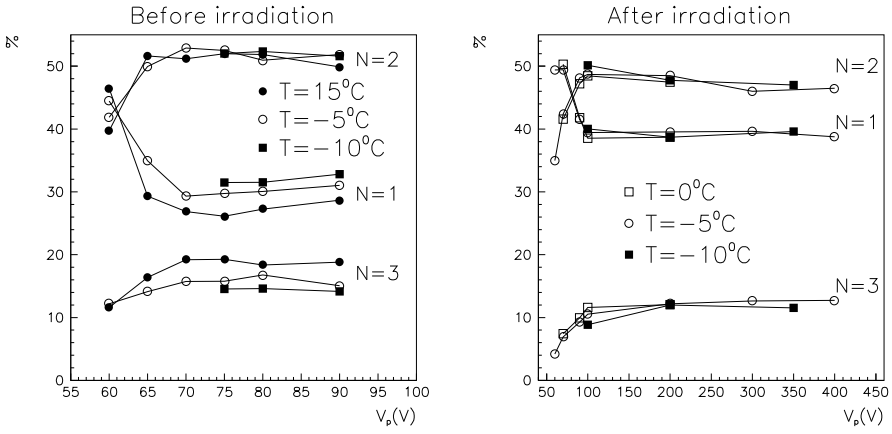


(a) (b)

Figure 8: Fraction of 1-, 2- and 3-strip clusters before irradiation (a) and after irradiation (b).

In order to have a better understanding of S/N values, we have evaluated $S_{cl}/N_{cl}$ separately for particles impinging on the detectors close to read-out or non-read-out strips. The impact position was determined by extrapolating the particle tracks reconstructed by the telescope. Only those events were considered in which the particles crossed the detector within 15 $\mu m$ from a read-out or a non-read-out strip, in order to be confident in the samples purity (see following paragraph). The measured and simulated S/N values are compared in table 3.

We also investigated the influence of the read-out pitch on $S/N$ ratio. For 224 $\mu m$ read-out pitch $S_{cl}/N_{cl}$ was found to be lower than for 112 $\mu m$ read-out pitch: $S/N \simeq 11$ before irradiation and $S/N \simeq 8.2$ after irradiation, at $T = -5\,^{\circ}C$ and $V_p = V_{dep} + 20\,V$, to be compared to $S/N \simeq 13$, $S/N \simeq 12$, respectively, for 112 $\mu m$ read-out pitch in the same conditions.

| | Before irradiation | | After irradiation | |
|---|---|---|---|---|
| | readout | not-readout | readout | not-readout |
| Simulation | 13.5 | 10.9 | 14.2 | 9.5 |
| Measurement | 14.2 | 11.1 | 14.7 | 11.5 |

Table 3: Comparison of simulated and measured signal-to-noise ratios for 112 $\mu m$ read-out pitch.

## 5.2 Cluster size

The particles crossing our detectors, characterized by a physical strip pitch of $p_f = 56\ \mu m$, induce signal on one or two read-out strips in $\simeq 90\%$ of the cases. The 1-strip clusters can be associated mostly to particles impinging near a read-out strip, while 2-strip clusters to an impact close to a non-read-out strip, since in this latter case the charge is coupled to the two neighbouring read-out strips. The relative abundance of 1- and 2-strip clusters depends mostly on the strip pitch and on the diffusion lenght of the induced electrons, $\lambda_{diff}$, but also on the capacitive couplings between the strips. In first approximation, we can assume that the charge is collected, with high probability, by a read-out strip (1-strip clusters) if the distance between the impact point and the strip is less than s/2, with $s = p_f - \lambda_{diff}$, and collected by a non-read-out strip (2-strips clusters) if the impact is outside this region [9]. For our detectors, before irradiation, $\lambda_{diff}$ can be estimated to be $15\ \mu m$ [11], so that the ratio of these two regions is 0.58. This is in good agreement with the measured relative fractions of 1- and 2-strip clusters (figure 8-(a)). If the charge of the cluster is high enough the signal may be coupled to further strips giving 3- or 4-strip clusters, even if with a much lower yield. After irradiation the ratio of the number of 3- or 2-strip events to the number of 1-strip events is smaller. This can be attributed to the lower interstrip capacitance, which results into a less effective charge coupling. No appreceable cluster size variation has been observed,within the studied temperature range, for the irradiated detectors(figure 8-(b)).

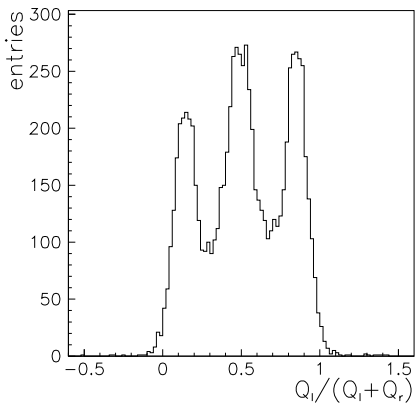


Figure 9: Distribution of the response function $\eta$.

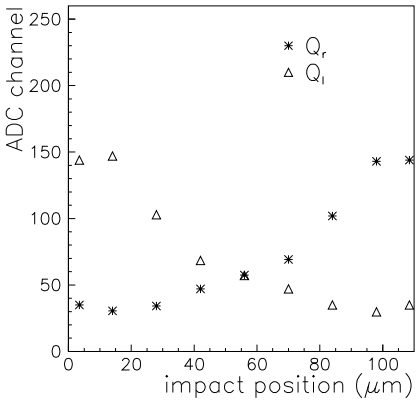


Figure 10: $Q_l$ and $Q_r$ as a function of impact position in the case of 2-strip clusters.

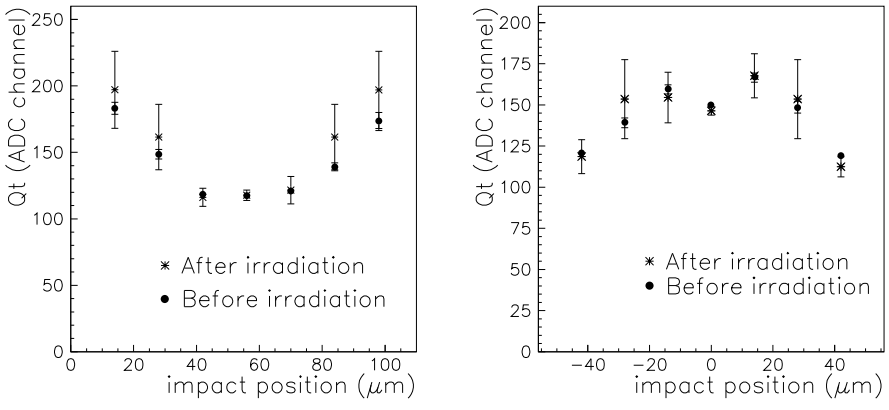


(a) (b)

Figure 11: Total charge as a function of impact position before and after irradiation ($T = -5\ ^{\circ}C$, $V_p = V_{dep} + 20\ V$) for 2-strip events (a) and for all events (b). The 0 position corresponds to a read-out strip.

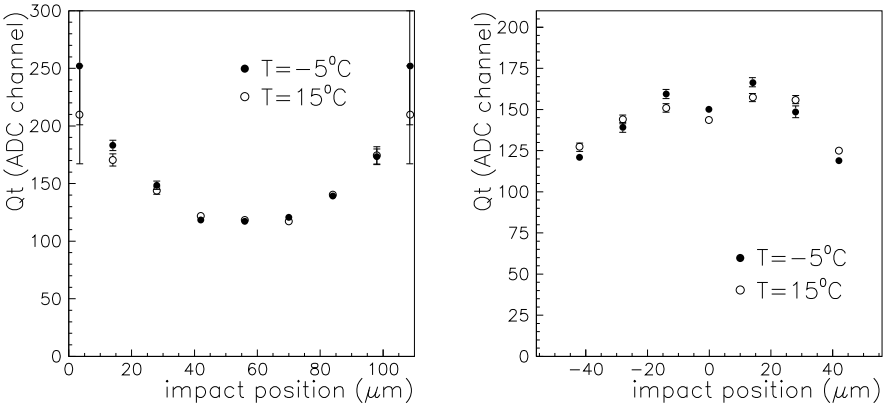


(a) (b)

Figure 12: Total charge as a function of impact position at different temperatures ($V_p = V_{dep} + 20\ V$) before irradiation, for 2-strip events (a) and for all events (b). The 0 position corresponds to a readout strip.

## 5.3 Charge collection

The total charge collected by a microstrip detector is only a fraction of the charge produced by the particle inside the detector. This fraction depends on the coupling between the strips and the read-out electronics. Since read-out and non-read-out strips have different couplings, the collected charge depends on the impact position of the particles. In order to study this effect, the charge on the two closest (left and right) read-out strips to the impact point, $Q_l$ and $Q_r$ was evaluated. The impact position on the detectors was determined using the particle tracks reconstructed by the telescope, which was precisely aligned to the test module. Only those events were considered for which the difference between the extrapolated (telescope track) and the measured (determined by the center of gravity of the strip charges) impact point was less than the variance of the respective distribution.

The distribution of the response function $\eta = Q_l/(Q_l + Q_r)$ is shown in figure 9; it is nearly simmetrical, as expected. The peak at $\eta = 1/2$ is due to the presence of non-read-out strips. The distribution of $Q_l$ and $Q_r$ versus particle impact position are also simmetrical, as shown in figure 10, where 0 and 112 $\mu m$ impact positions correspond to the location of the two read-out strips, while impacts at 56 $\mu m$ to that of the non-read-out strip.

In figure 11-(a) the total charge, $Q_t = Q_l + Q_r$ in the case of 2-strip clusters only is compared before and after irradiation at $T = -5°C$. Because of the worse coupling, the total charge is less if the particle hits the detector close to a non-read-out strip than if it hits the detector close to a read-out strip. The normalised total charge for all clusters is shown in figure 11-(b). Since particles crossing the detector close to a readout strip produce mainly 1-strip cluster, the points at impact position 0 in figure 11-(b) correspond, practically, to 1-strip cluster events. The normalized total charge as a function of the impact position does not show significant differences before and after irradiation and at different temperatures (see figures 11 and 12).

By dividing the total charge value obtained for particles impinging on non-read-out strips by the one measured for particles impinging on read-out strips we could estimate the relative charge collection efficiency. These ratios were also evaluated by simulation [3], and are compared in table 4.

| $Q_t^{not-readout}/Q_t^{readout}$ | measurement | simulation |
|---|---|---|
| before irradiation ($T = -5°C$) | 0.76 | 0.80 |
| after irradiation ($T = -5°C$) | 0.76 | 0.67 |

Table 4: Relative charge collection efficiencies.

We also studied the charge collection efficiency in the case of 224 $\mu m$ read-out pitch, when only every second read-out strip was connected to the read-out electronics. The simulation shows that in this case the signal loss is significantly larger [3]. When the signal is induced onto a connected read-out strip the charge coupling efficiency to the readout electronics is 93% (94%) before (after) irradiation, and there are mainly 1-strip clusters events. If the signal is induced on a disconnected read-out strip the coupling efficiency falls down to 51% (41%), and the charge is shared equally on the two neighbouring connected read-out strips. In this case, 2-strip clusters events are

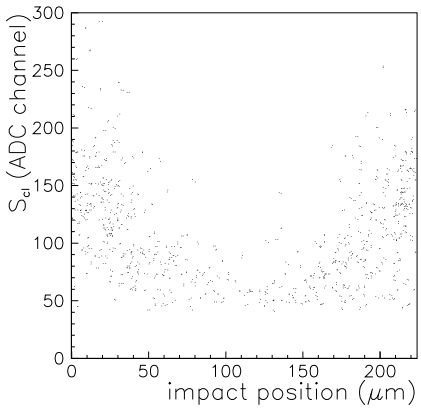


Figure 13: Cluster signal distribution as a function of impact position for 1-strip clusters. The 0 and 224 $\mu m$ positions correspond to read-out strips connected to the electronics, 56 $\mu m$ and 168 $\mu m$ to non-read-out strips, while 112 $\mu m$ to a not connected read-out strip.

to be expected. Finally, applying the signal to a non-read-out strip 47% (38%) of the injected charge is induced on the closest connected read-out strip and 12% (9%) on the farther connected read-out strip. The signal expected on the farther read-out strip is comparable to the noise level ($\simeq 10$ ADC counts) and, therefore, in most of the cases it doesn't survive the selection cuts, so that the resulting events are mainly consisting of 1-strip clusters.

These effects have been observed in real data, as can be seen in figure 13 and 14. In figure 13 the cluster signal of 1-strip events is plotted as a function of the impact position. If the impact is close to the read-out strip the signal is high. If the particles cross the detector close to a non-read-out strip the signal reduces to about one half its maximum. Close to a not connected read-out strip there fall just few events, with very low signals, since most of the events are made of 2-strip clusters in this case.

In figure 14 the cluster signal distribution for 1-, 2-strip clusters and for all clusters can be seen before and after irradiation. The signal amplitude distributions for 1-strip events exhibits, as was already evident in fig. 13, two well separated peaks. The peak at larger signal amplitudes is due to events in which the particle impact is close to a connected read-out strip, while the peak at smaller amplitudes to events in which the particle crosses the detector close to a non-read-out strip. The ratio between the peak value of the 2-strip cluster signal and the highest peak value of the 1-strip cluster signal is 0.75 (0.61) before (after) irradiation, while the ratio between the two peak values for the 1-strip cluster signal is 0.53 (0.44). These results are in agreement with the simulated values, thus supporting our qualitative explanation.

The results obtained for not connected read-out and non-read-out strips indicate that the strip pitch of the detector cannot be further increased much above the present 112 $\mu m$ value without losing efficiency.

## 5.4 Spatial resolution

We also tried to evaluate the detectors spatial resolution, even if the low statistics of available data did not allowed us to optimize the selection cuts for this study. The resolution of the detector was determined from the standard deviation ($\sigma_{res}$) of the residual distribution. The residual is the distance between the reconstructed (by the telescope) track position on the detector and the center of gravity of the cluster. The intrinsic spatial resolution $\sigma_{in}$ was calculated from:

$$\sigma_{in} = \sqrt{\sigma_{res}^2 - \sigma_{tel}^2 - \sigma_c^2},$$

where $\sigma_{tel}$ is the spatial resolution of the telescope and $\sigma_c$ is the variance of the impact position due to the multiple Coulomb scattering. Since the particle energy was $100\ GeV$, where the Coulomb scattering is negligibly small, we did not take into account $\sigma_c$, while $\sigma_{tel}$ was estimated to be $8\ \mu m$ [8].

The resolution obtained for not irradiated and irradiated detectors can be seen in table 5 at $V_p > V_{dep}$ and $T = -5°C$. No significant change of the resolution have been observed for the irradiated detector within the statistical errors. We found that the resolution does not depend on the bias voltage after full depletion in both irradiated and not irradiated case.

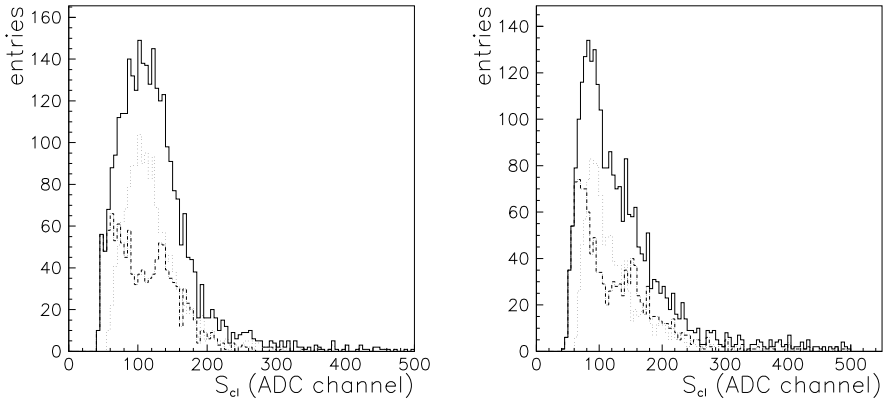


(a) (b)

Figure 14: Signal amplitudes distributions before (a) and after (b) irradiation. Solid line: all events; dashed line: 1-strip events; dotted line: 2-strip events.

| | $\sigma_{in}$ |
|---|---|
| before irradiation | $21.8 \pm 0.7 \mu m$ |
| after irradiation | $22.2 \pm 1.3 \mu m$ |

Table 5: Detectors spatial resolution before and after irradiation

## 5.5 Efficiency

The hit efficiency is defined as the ratio between the number of clusters in which the track extrapolated from the telescope matches the hit position on the detector (cluster center of gravity) and the total number of tracks. A cluster is defined to match the extrapolated track if its position is within a region of $112\ \mu m$ around the predicted position. We measured the efficiency selecting detectors regions free of noisy channels and in which the beam profile was uniform.

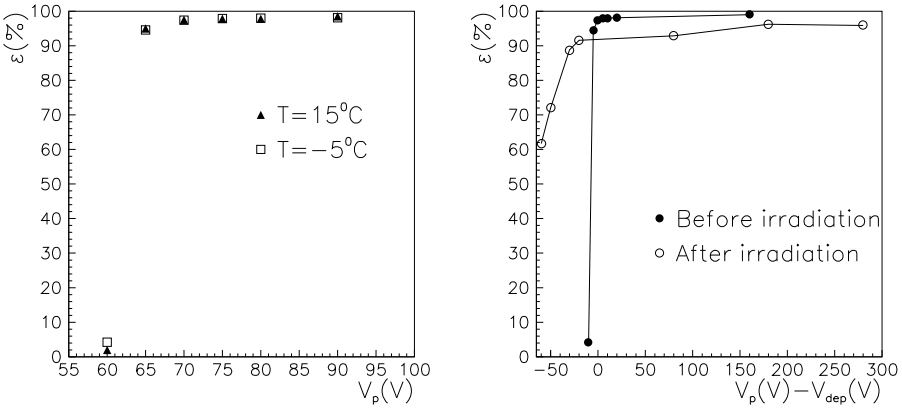


(a) (b)

Figure 15: Detector efficiencies at -5 and 15 $^{\circ}C$, before irradiation (a); before and after irradiation, at -5 $^{\circ}C$ (b).

Figure 15 shows the efficiency as a function of the depletion voltage, before and after irradiation. Above full depletion the efficiency, independently from the temperature, reaches $98\%$ before irradiation and $96\%$ after irradiation. Below the depletion voltage the efficiency of the irradiated detectors decreases slowly with decreasing bias voltage, while it falls much faster to zero in the case of unirradiated detectors. This is the consequence of type inversion, as discussed above. It is important to emphasize that this kind of detectors, after irradiation, still have an efficiency

of about 70 % at 50 $V$ below the full depletion voltage.

# 6 Conclusions

We tested, with high energy particle beam, $n^+$ on $n$ type silicon microstrip detectors before and after neutron irradiation. The detectors were irradiated at a fluence of $8.3 \times 10^{13}\ n/cm^2$. The signal-to-noise ratio of a module, with 11.48 $cm$ strip lenght and 112 $\mu m$ readout pitch, was around 13 for irradiated devices. The charge division, the detectors efficiency and spatial resolution were also very similar before and after irradiation and, in general, we have found that their performances do not worsen significantly after irradiation if high enough bias voltage is provided.

The main advantage of this kind of detectors have been confirmed: after type inversion has occured, at 50 $V$ below the full depletion voltage there is only $20 \div 30\,\%$ degradation of signal-to-noise ratio and efficiency, while standard $p^+$-on-$n$ type detectors cannot work in the same conditions. However, the $S/N$ ratio of this detector, essentially due to the high interstrip capacitance, is lower than that of $p^+$-on-$n$ devices with the same pitch and strip lenght for both not irradiated and irradiated devices, for which $S/N$ values around 22 and 17, respectively, have been measured [1].

# Acknowledgements

We express our thanks to the CMS collaboration for inspiring and supporting our work. We in particular thank B. Schwaller, F. Drouhin, A. Giassi, P. G. Verdini for their work in the DAQ group, and among our technicians G. Sala for his contribution to the electrical characterization measurements, R. Ferorelli and P. Cariola for designing and realizing the mechanical structure. We are also grateful to SINTEF and to the ATLAS collaboration for permitting us to use and test their prototype detectors.

# References

[1] CMS, The Tracker Project, Technical Design Report, CERN/LHCC 98-6 CMS TDR (1998).

[2] M. M. Angarano, A. Bader, D. Creanza, M. de Palma, D. Diacono, S. My, G. Raso, P. Tempesta, *Characteristics and SPICE simulation of a single-sided, $n^+$ on $n$ type Si strip detector before and after neutron irradiation*, CERN CMS NOTE 1998/34.

[3] A. Bader *et al.*, *Signal-to-noise simulation of an $n^+$ on $n$ type Si microstrip detector*, CERN CMS NOTE 1998/13.

[4] SINTEF,http://www.oslo.sintef.no

[5] ATLAS Technical Design Report, CERN/LHCC/97-17 (1997)

[6] The ATLAS Prototype Detector, SINTEF, http://www.oslo.sintef.no/ecy/7230/atlas.html.

[7] L. L. Jones, *Premux128 specification*, version 2.3 (1995).

[8] L. Celano *et al.*, *A hight resolution beam telescope built with double sided silicon strip detectors*, NIM A381 (1996) 49-56.

[9] D. Adriani *et al.*, *Beam test results for single- and double-sided silicon detector prototypes of the CMS central detector*, NIM A396 (1997) 79.

[10] Kalbfleisch *et al.*, *Charge sharing and resolution studies of double-sided silicon microstrip detectors with boron spray implants*, NIM A355 (1995) 366-385.

[11] A. Peisert, *Silicon microstrips detector, in experimental techniques in high energy physics*, F.Sauli, Addison-Wesley, 1987.

[12] Turchetta *et al.*, *Spatial resolution of silicon microstrip detectors*, NIM A335 (1993) 44-58.

[13] A. Candelori, A. Paccagnella, F. Nardi, A. Bacchetta and D. Bisello, *SPICE evaluation of the S/N ratio for Si microstrip detectors*, before publication.

[14] I. Stavitski, private communication.